N. Jb. Geol. Paläont. Abh. 298/1 (2020), 17–33
Stuttgart, October 2020

Article

The origin of the serpentinite enclaves in metacarbonates of the Sa Nghia area in the Kon Tum Massif, Central Vietnam

Wojciech Smoliński, Lucyna Natkaniec-Nowak, Wiesław Heflik, Giang Nguyen Khac, Piotr Gunia, Magdalena Dumańska-Słowik, and Ban To Xuan

With 7 figures and 3 tables

Abstract: Metacarbonate rocks surrounded by schists, amphibolites and quartzites, occur abundantly in the Sa Nghia – Ho Moong area of Kham Duc Complex in the Kon Tum Massif (Central Vietnam). They contain serpentinite enclaves, which form different bodies such as: sharp-edged rock fragments, lenses, thin layers or small nests often transecting the background of host metacarbonates. The enclaves are mainly built of antigorite. Thin veins crosscutting the serpentinites are commonly filled with microcrystalline carbonates. The relics of olivine and clinopyroxene as well as flaky talc, magnetite, ilmenite, pyrite and zircon occur as accessory components. The serpentinites are slightly enriched in Cs, Th and U, and depleted in Ba, K and Ti. Most probably, such geochemistry could be caused by the influence of fluids derived from primitive tholeiitic melt, which could infiltrate the primary ultramafic rocks before they were hosted by metacarbonates. Another alternative is that the impoverishment in Al, Cr, Ni, Cu, V and Co, together with the presence of numerous grains of carbonates, zircon and pyrite might be indicative for significant secondary metasomatic alterations of pristine ultramafic rocks as the protolith of the serpentinite enclaves.

Key words: Serpentinites, metacarbonates, metasomatism, Kon Tum Massif, Central Vietnam.

1. Introduction

Serpentinites are alteration products of different types of rocks enrich in magnesium (Posukhova et al. 2013). These rocks are found in almost all continents of the Earth (e.g. Coleman 1977; Yang & Seccombe 1993; Fryer et al. 1999; Azer & Khalil 2005; Gunia 2005; Cannat et al. 2010; Hirth & Guillot 2013). Guillot & Hattori (2013) suggested that more than 3% of the Earth's surface is made of these rocks together with peridotites.

In northern Vietnam serpentinites occur in several areas such as: Nui Nua (Thanh Hoa), Pho Rang (Lao Cai), Ban Phuc (Son La) and Suoi Giang (Yen Bai). Some of them are also located in central part of the country, i.e.: Hiep Duc, Lang Hoi (Quang Nam) and Sa Nghia (Kon Tum Massif). In the latter locality serpentinite enclaves were identified within metacarbonate rocks (Mg-marbles) between Nghia Ta Village of Sa Nghia Commune and Tan Sang Village of Ho Moong Commune in Sa Thãy district (14° 27′ 01.6″ N, 107° 50′ 20.1″ E) by geologist from the Hanoi University of Mining and Geology in Vietnam. This region was investigated with boreholes as well as other geological and hydrogeological survey. Serpentinites found there form small bodies within metacarbonate rocks at a depth of several to several dozen meters. Locally they occur also on the surface of this area. These serpentine enclaves exhibit various mesostructures and forms, such as: sharp-edged, brecciated fragments, irregular areas with many parallelly oriented thin layers, bodies resembling glomero- and cumuloblasts transected by frequent serpentine-bearing veins or microcrystalline carbonate assemblages with "patchy" appearance. In the world literature, data on metacarbonate rocks and serpentinites from this region is very

DOI: 10.1127/njgpa/2020/0930

www.schweizerbart.de
0077-7749/2020/0930 $ 4.25

limited. Only scarce information was provided on occasional use of these rocks (serpentinites, phlogopite-bearing marbles), mainly as a decorative material for local handicraft workshops (Giang et al. 2013).

In the Sa Nghia–Ho Moong area, being a part of the Kham Duc Complex in the Kon Tum Massif, metacarbonates with different serpentinite bodies are found between schists, amphibolites and quartzites. Based on the genetic features, Huynh et al. (2009) and Giang et al. (2013) divided these rocks into two groups, i.e. metamorphic and metasomatic types. The metamorphic varieties are represented by phlogopite marbles (metacarbonates) interbedded with small lenses of quartz-biotite-bearing amphibolites. To the metasomatic group, which occur mainly in the Kham Duc Complex, belongs: phlogopite-serpentine- and cal-silicate-bearing rocks, also calcite-silicate metasediments (i.e. olivine marbles, olivine-pyroxene marbles) as well as monomineral wollastonite varieties and serpentinized ultramafics of peridotite type. Into the last genetic group were included also such varieties of phlogopite marbles, which underwent intensive metasomatic alterations (Huynh et al. 2009; Giang et al. 2013).

As it was revealed from petrological data, the phlogopite-serpentine-bearing rocks forms small, a few meters long and up to 0.5 m thick pots and lenses, which often contain, in addition to phlogopite and serpentine-group minerals, also: calcite, dolomite, talc, tremolite and opaque minerals. The calcium-silicate and carbonate-silicate zones are composed mainly of calcite, olivine, diopside, wollastonite, with small nests and lenses of serpentinites. In the Sa Nghia–Ho Moong area, these serpentinite bodies are ranging from 0.1 to 0.5 m in size and contain mainly serpentine, wollastonite and relics of strongly crushed olivine and pyroxene. According to Huynh et al. (2009) and Giang et al. (2013), all the Sa Nghia–Ho Moong metacarbonates can be interpreted as metamorphosed clay and lime-clay sediments, as well as scarce mafic rocks. These authors also claim, that serpentinites found in enclaves within the metacarbonates could be a product of carbonate involving reactions.

The main aim of this work was to provide the detailed petrology and description of textural relationships in serpentinites enclaves found in the metacarbonates from the Sa Nghia area (Sa Thầy district). The microscopic data were supported by the whole-rock geochemistry to discuss the genesis of these bodies, and reconstruct the relative time sequence of the events during their tectono-metamorphic history.

2. Geological settings

Central part of Vietnam, as well as the neighbouring countries, i.e.: Laos, Cambodia, western Thailand, as well as the south-eastern part of the Malayan Peninsula, and certain fragments of Sumatra and Borneo, belong to the Indochina plate (Metcalfe 1984, 1988, 1994, 1996, 1998 2000; Golonka et al. 2006). The Khorat Block with Kon Tum Massif, i.e. its main structural unit, occurs in the core part of this plate (Phan Truong Thi 1978; Brookfield 1996). The Kon Tum Massif represents the largest continuous exposure of crystalline basement of the Indochina craton (Fig. 1A), regarded as stable continental core of South-East Asia (Hutchison 1989; Lan et al. 2003). According to Maluski et al. (2005), it is an old fragment of Gondwana (as a stable Precambrian basement), built of metamorphic rocks, similar to the rocks found in Southern India and Antarctica (e.g. Katz 1993; Lan et al. 2003).

The Kon Tum Massif is located in the southern part of Trans Vietnam Orogenic Belt (TVOB), a region formed due to the collision of two cratons, i.e. South China and Indochina (Nakano et al. 2009; Owada et al. 2016). The massif is mainly composed of Precambrian rocks intensively altered during tectono-thermal events from Ordovician-Silurian to the Late Permian-Early Triassic periods, into: schists, gneisses, amphibolites and quartzites (e.g. Tran 1998; Nagy et al. 2001; Osanai et al. 2004; Owada et al. 2016). These metamorphic rocks are partly covered by Mesozoic volcano-sedimentary formations (Carter et al. 2001; Lepvrier et al. 2004) and Neogene ± Quaternary basaltic cover. Locally the rocks are intruded by Paleo-Mesozoic granodiorite bodies (Pham Trung Hieu et al. 2016). The Kon Tum Massif is cut by a series of faults with a variable course, that divide it into smaller geological units (Fig. 1B), i.e.: Kham Duc Complex (north and western part), Ngoc Linh Complex (central-western) and the Kannak Complex (central-eastern) (e.g. Hai 1986; Trinh Van Long 1995; Osanai et al. 2003). The Kham Duc Complex is mainly built of metamorphic rocks, i.e.: hornblende-biotite gneisses, epidote amphibolites, quartzites, biotite-muscovite schists, biotite-sillimanite schists, low-temperature and medium pressure schists (Nakano et al. 2007a, b). Locally, kyanite-talc and zoisite-crossite schists, marble and metacarbonate lenses also occur in this area (Trinh Van Long 1995).

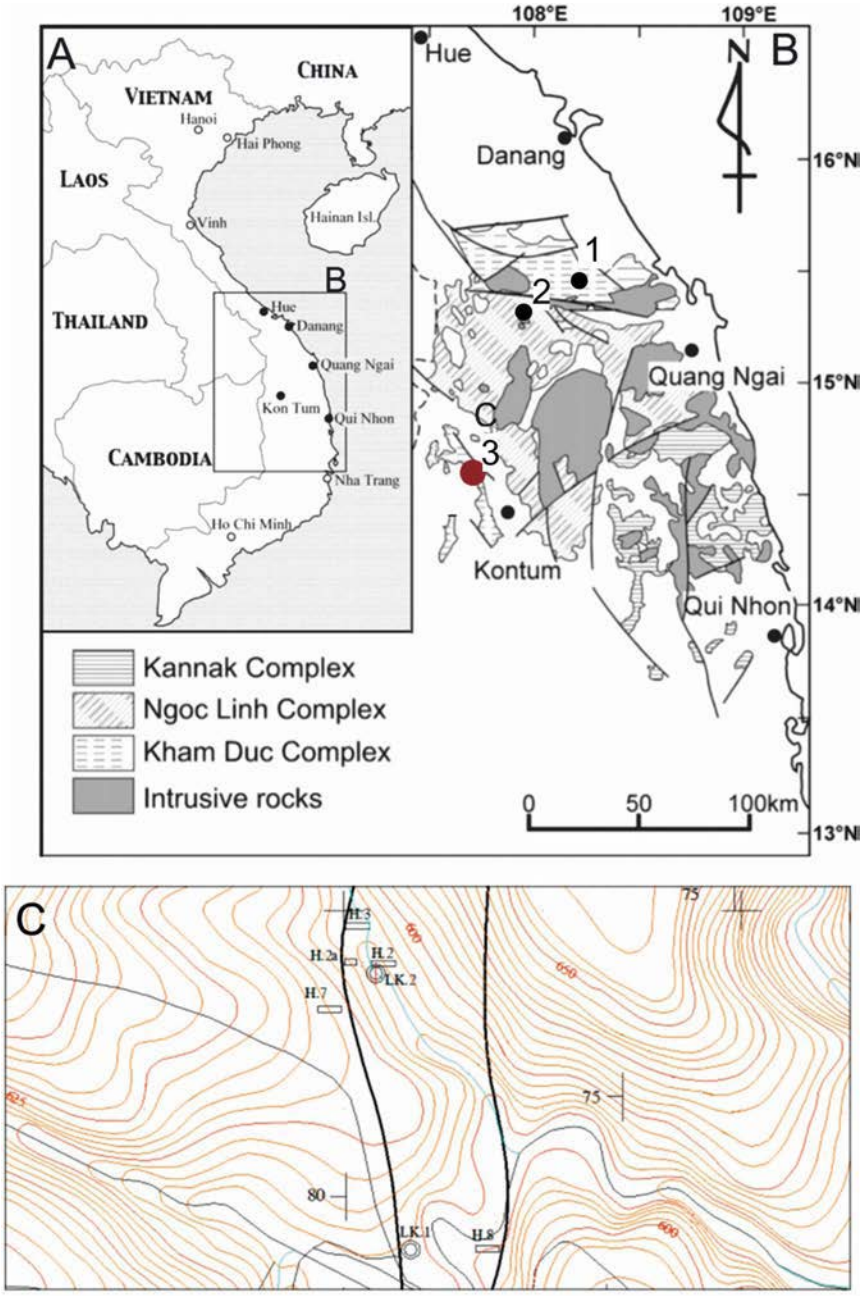

Fig. 1. A. Geologic sketch of the study area in Central Vietnam; B. Geologic map of Kon Tum Massif (compiled after United Nations 1990; Osanai et al. 2004; Nakano et al. 2007) with the location of serpentine occurrences: 1 – Hiep Duc, 2 – Lang Hoi (Quang Nam), 3 – Sa Nghia; C. Location of two boreholes (LK1 and LK2) in Sa Nghia-Ho Moong area.

3. Materials and methods

The samples of serpentinites were collected from two boreholes LK1 and LK2 and from one outcrop on surface (sample SH.203). The distance between the boreholes LK1 and LK2 is 145 m (Fig. 1C). In LK1 borehole samples were collected at the depths of 14, 20, 56, 60, 61, 64 and 67 m below ground level (bgl) while in LK2 borehole at the 10 and 40 m bgl. Four samples of metacarbonates (LK1/67, LK1/64, LK1/20, LK1/14) and six samples of serpentinites (LK1/56, LK1/60, LK1/61, LK2/10, LK2/40, SH.203) were examined by polarizing microscope, scanning electron microscope and

Raman micro-spectroscopy. The bulk-rock trace and REE chemistry data were interpreted using different discrimination diagrams.

Petrographic characteristics of thin sections were made under transmitted light using an Olympus BX 51 and BA310POL polarizing microscopes with a magnification range from 40× to 400×. Backscattered electron observations (BSE) were performed on polished, carbon-coated sections using an FEI Quanta 200 Field Emission Gun scanning electron microscope equipped with energy-dispersive X-ray spectrometer (EDS). The system was operated at 20 kV accelerating voltage in a high-vacuum mode.

Raman vibrations spectra of selected minerals from serpentinites were recorded using a Thermo Scientific DXR Raman microscope under 10×, 50× and 100× magnification with automatic "x-y" table. Before Raman analyses were made the planes of thin sections and cleavage surfaces were clean with acetone. The samples were excited in room temperature with the 532 nm laser, with focus diameter about 1–2 mm, and laser power range of 5–10 mW. The RS spectra were corrected for background by a sextic polynomial method using Omnic software.

The whole-rock analyses of serpentinites were carried out in the Bureau Veritas Mineral Laboratory, Vancouver, Canada. The abundances of major oxides and trace elements were determined using Inductively Coupled Plasma-Optical Emission Spectrometry (ICP-OES) and Inductively Coupled Plasma-Mass Spectrometry (ICP-MS) after a fusion of powdered samples in lithium metaborate/tetraborate and dilution of nitric digestion. Major oxides and trace elements were determined using Thermo Jarrell-Ash ENVIRO II ICP or a Spectro Cirros ICP and Perkin Elmer SCIEX ELAN 6000 ICP-MS apparatus, respectively. Calibration was made using multiple United States Geological Survey (USGS) and Canada Centre for Mineral and Energy Technology (CANMET) certified reference materials.

4. Petrography of host metacarbonates

Metacarbonates from the LK1 borehole (LK1/67, LK1/64, LK1/20, LK1/14) are pale green-grey in colour and frequently intersected with small white veins. They are characterized by the presence of many microtextures and frequent assemblages of various opaque ore minerals differing in size and forms of occurence. The rock samples from the deepest parts of the borehole LK1 profile (e.g. LK1/67 and LK1/64) have a distinct schistosity, with the alternating fine-grained dolomite and coarse-grained serpentine-bearing laminae. In terms of composition, they seem to correspond to the carbonate-silicate rocks distinguished by Huynh et al. (2009) and Giang et al. (2013). In the coarse-grained veins the elongated antigorite laths dominate over other serpentine-group minerals. Locally, they form radiant assemblages (sample LK1/67) with admixture of secondary fibrous chrysotile (sample LK1/64). In some cases serpentine background is locally intersected by youngest veins filled with coarse-crystalline dolomite. The well visible laminated texture indicates, that serpentine-group minerals could formed as a result of the widespread deformation after the transformation of the clay carbonate, pyroclastic and ultramafic protolith under conditions of low-grade regional metamorphism.

The other sample from shallower depths of LK1 borehole (LK1/20) has grano-lepidoblastic and unoriented massive texture. It is mainly composed of calcite, which make up ca. 60–70 vol.%, while serpentine, amphibole (tremolite/actinolite), brucite, talc and phlogopite occur only in subordinate quantities. The results of microscopic observations enabled to recognize two forms of carbonate component in the rock-background. Fine-crystalline calcite, which makes up the main rock mass, is the most widespread mineral. The second type of carbonate is coarse-grained, with well-marked traces of rhombohedron faces. It is often transacted by thin veins filled with brucite. Moreover, the irregularly scattered chrysotile accompanied by talc flakes are found in the calcite mass. Tremolite, phlogopite and pyrite occur only as accessory components in this rock. The obtained result of petrographic studies indicates, that composition of this sample is similar to the phlogopite-serpentine and calcite-silicate rocks from Kon Tum Massif described earlier by Huynh et al. (2009) and Giang et al. (2013). Its mineral composition and structural features might evidence the dynamic event of regional metamorphism connected with strong shearing deformation.

The LK1/14 sample represents an unique brecciated fragment which rock-background is composed of different types of minerals. In many places, it is crosscut by a several systems of very fine veins. Their fine-crystalline groundmass contains mainly calcite with traces of actinolite, phlogopite and talc. Serpentine-group minerals (chrysotile and lizardite) form fibrous or lathy assemblages differing in size, often included in carbonate groundmass. Wollastonite and actinolite occur as large elongated crystals (about 5.0 mm long), often cracked and filled with calcite, talc and/or serpentines. Brucite forms small aggregates of flakes and laths, or occur as fillings in thin veins. Garnet (hydrogarnet?) seems to be the accessory component of wollastonite+brucite+actinolite association. It form an isometric grains with isotropic optical character, and sizes up to 2.0 mm. Pyrite forms numerous, large euhedral and anhedral crystals, even up to 4.0 mm in size.

Among the other accessory components magnetite, rutile and zincite have been determined. Generally, the LK1/14 sample could be assigned to the calcite-silicate type, devined by Huynh et al. (2009) and Giang et al. (2013).

5. Petrography of the serpentinite enclaves

5.1. Microscopic observations

All serpentinite samples from two boreholes of LK1 (LK1/56, LK1/60, LK1/61) and LK2 (LK2/10, LK2/40), as well as the outcrop – sample SH.203, exhibit very similar macroscopic features. They are dark to light green in colour, with occasionally visible small white or black patches. Under microscope, the samples show flame-shaped, interlocking or interpenetrating texture. In most cases, the rocks have weakly- to moderately-oriented and massive texture. The rocks background is frequently intersected with numerous veins filled with serpentine flakes or fibres, fine grained carbonates and opaque magnetite microspherules.

Serpentine-group minerals make up the background of analytical rocks from 40 to 95 vol.%. They are most often represented by antigorite, whereas lizardite and non-asbestos chrysotile occur in small amounts. Antigorite blades form mostly interpenetrating intergrowths within the rock mass. Lizardite and chrysotile fill veins in antigorite background and sometimes occur as cell-shaped forms (Fig. 2A). At least two generations of serpentine-group minerals can be distinguished, i.e., (1) tabular, lamellar and platy crystals making up the main mass of the rock-background, and (2) thin needle-like crystals found in the interstices between them. Locally, the relicts of primary olivine and pyroxene are found within serpentine groundmass (Fig. 2C, D). Carbonates are mainly represented by calcite and dolomite (30–60 vol.%). They form very small to large crystals, varying between 50–500 µm in size, filling veins of the serpentine groundmass (Fig. 2E). Frequently they are significantly penetrated by lamellar antigorite assemblages. Some idiomorphic carbonate individuals are strongly deformed and fractured. Talc and Ca-Mg amphiboles are quite rare. Talc occurs as plate-like crystals forming massive aggregates which coexist with carbonates and serpentines (Fig. 2F). Tremolite-ferroactinolite amphiboles form flattened, needle-shaped individuals coexisting in close association with serpentine-group minerals and dolomite within the rocks. The isolated spinel grains forming wormy-like aggregates (Fig. 2G) and large pyrite individuals with magnetite inclusions (Fig. 2H) are found in these rocks as accessory components.

5.2. Scanning electron microscopy (SEM-EDS)

The results of SEM-EDS analyses show that Fe compounds (sulfides and oxides/hydroxides) are the most abundant among the ore minerals (Fig. 3). Fe sulfides (pyrite) occur as euhedral and anhedral isolated individuals, as well as locally form massive aggregates. They host small inclusions of Fe oxides/hydroxides and chalcopyrite, forming irregular, anhedral grains. Other ore minerals are represented by titanium compounds (ilmenite and rutile/anatase). Generally, all ore minerals occur in close spatial association with carbonates filling veins in serpentine groundmass. Phlogopite occurs as deformed hexagonal flakes with slight zoning which can be observed well in BSE images. It is often found in close spatial contact with numerous Fe oxides/hydroxides assemblages. Moreover, single anhedral grains of zircon (ca. 0.05 mm) were found within the serpentine-carbonate background.

5.3. Raman micro-spectroscopy (RS)

The presence of three serpentine-group minerals, i.e., antigorite, lizardite and chrysotile is well proved with Raman micro-spectroscopy (Fig. 4). Their three the most intensive RS bands found in the regions such as: 683–688, 376–385 and 228–230 cm^{-1} are attributed to symmetric stretching modes (vs) of the Si–O–Si linkages, v5 modes of the SiO_4 and vibrations of O–H–O groups, respectively. Antigorite has diagnostic bands at 1,043, 683, 524, 459, 376, 348 and 229 cm^{-1}. Lizardite has its marker bands at 688, 382, 228 cm^{-1}, whereas chrysotile manifests its presence by bands at 1,102, 688, 385, 350 and 230 cm^{-1}. Locally, in some rock samples, lizardite co-exists with brucite, which shows its two distinctive bands at 442 and 277 cm^{-1} attributed to A1g (T) and Eg (T) modes, respectively (Braterman & Cygan 2006).

Carbonates represented by calcite and dolomite, show a few prominent bands in their Raman spectra. Calcite has the most intensive band at 1,085 cm^{-1}

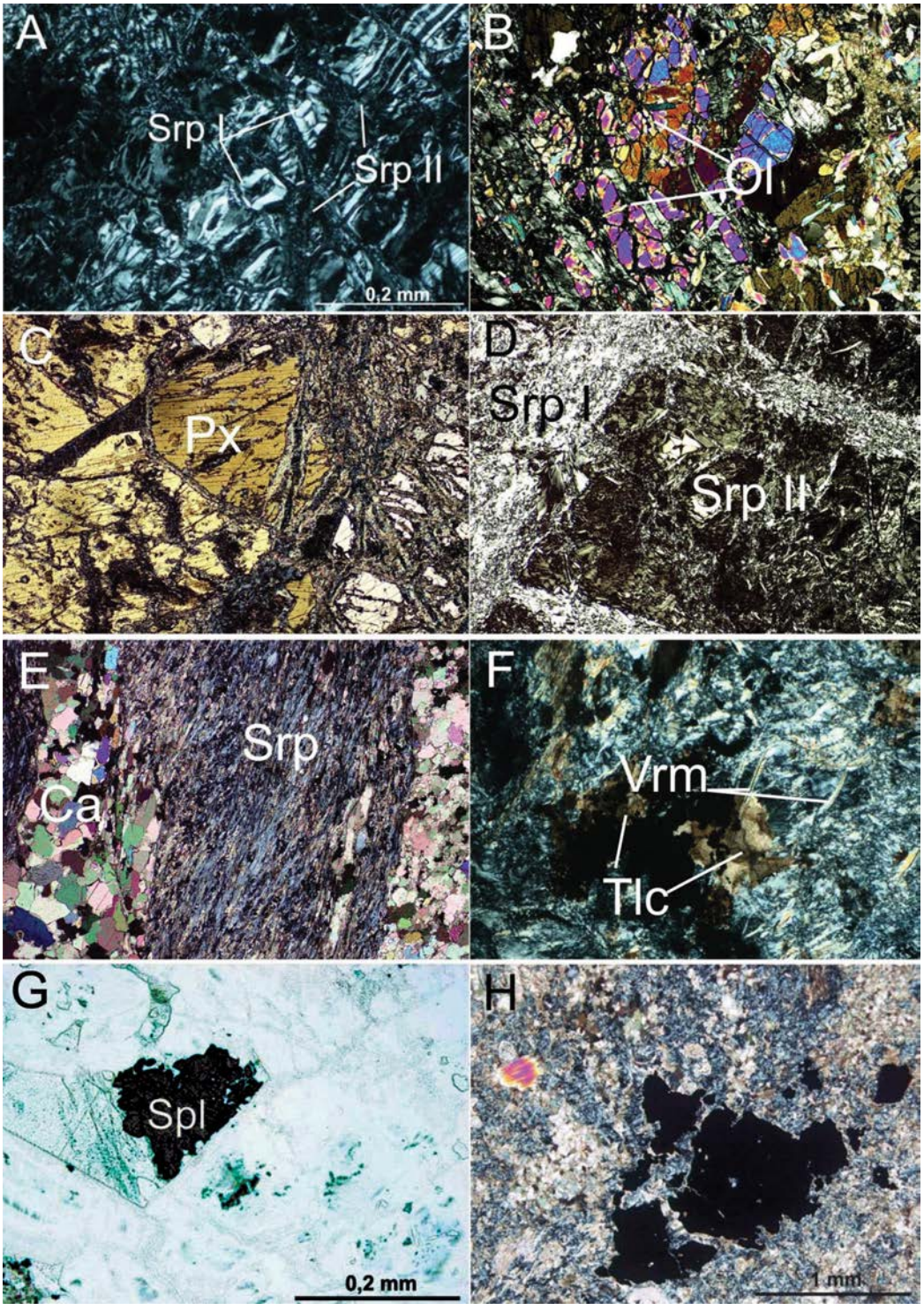

Fig. 2. A. Cell and hour-glass shapes of older structures of serpentine (Srp I) transecting by younger banded veins (Srp II); B. Cracked and shattered olivine relics (Ol) in the rock-background; C. Clinopyroxene prisms surrounded by narrow veins filled with fine-grained Mg-carbonates with vermiculite (?); D. Serpentine pseudomorph (bastite) after pyroxene (Srp II) surrounded by veins composed of felted (fibrous) chrysotile (?); E. Carbonate-amphibole rock with medium-grained calcite (Ca) transected by fibrous, parallelly oriented, chrysotile and tremolite intergrowths (Srp); F. Serpentine background with Mg-chlorite (and talc?; Tlc) disseminations and single blade-shaped vermiculite individuals (Vrm); G. Irregular, brownish, translucent accesory Cr-spinel in the antigorite serpentinite; H. Opaque magnetite after chromian spinels in surroundings filled of carbonate and serpentine minerals. Microphotographs with crossed nicols (except G). Samples: LK1/60 (A, B, C) LK1/61 (D, E) and SH.203 (F, G, H).

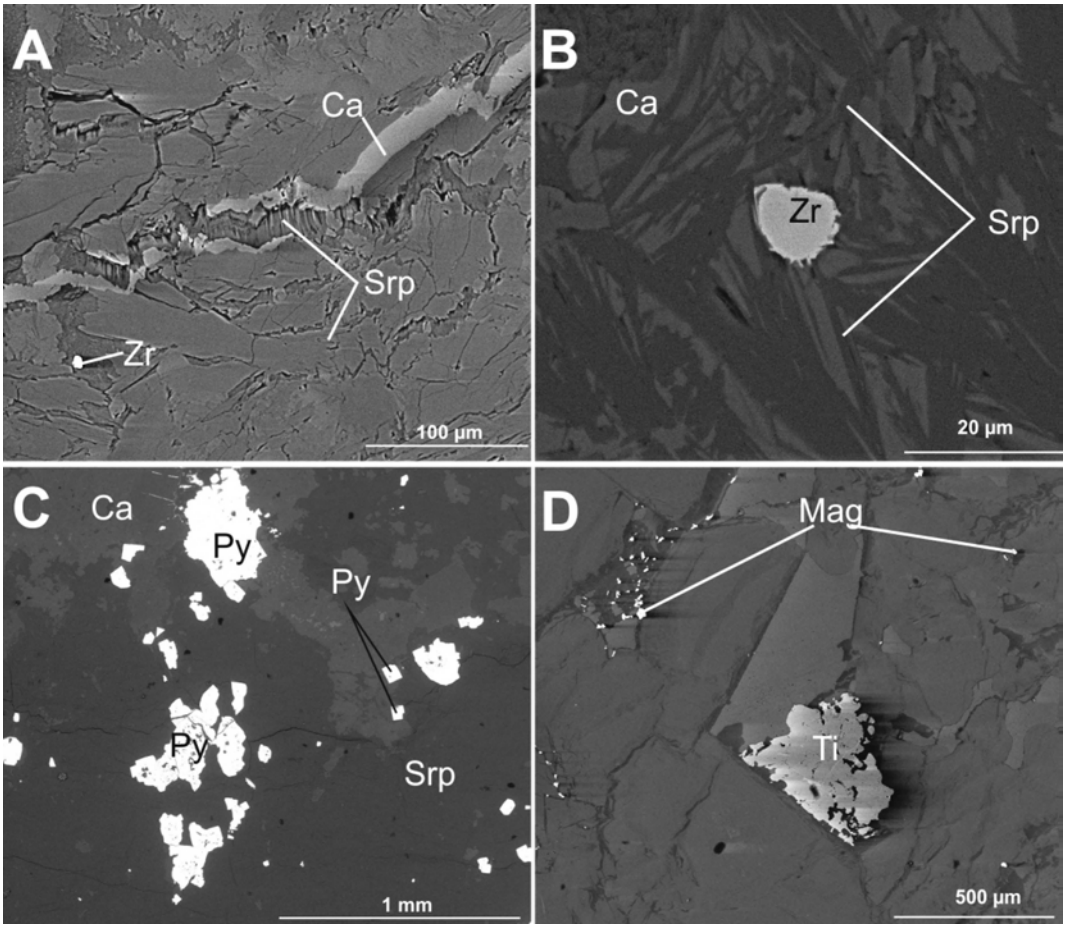

Fig. 3. A. Massive and asbestos-like serpentines (Srp), carbonate veins with "glassy" appereance and small oval zircon grain (Zr) in the rock background; B. Needle-like and blade-shaped crystals of antigorite accompanied by anhedral carbonates (Ca) and single zircon grain (Zr); C. Groups of anhedral crystals of pyrite (Py) cracked and filled by serpentine minerals (Srp); D. Cloudy elongated assemblages of very fine-sized magnetite microspherules and single anhedral crystal of ilmenite in the carbonate-serpentine background. BSE images of samples: LK1/61 (A, B) and SH.203 (C, D).

connected with ν1 symmetric stretching vibrations of CO_3 group. Other less intensive bands are found about 710 cm^{-1} attributed to ν4 symmetric deformation of CO_3, 280 and 153 cm^{-1} due to the relative translations between the Ca and CO_3 groups (Gunasekaran et al. 2006). The presence of dolomite is manifested by bands at 1,441, 1,097, 722, 298 and 174 cm^{-1}. Its diagnostic bands coming from ν1 and ν4 vibrations of CO_3 group, are shifted towards higher wavenumber at about 1,097 and 723 cm^{-1} than in calcite Raman spectrum. Similarly, the external modes due to translations between cations and anionic groups occur at wave numbers of 299 and 174 cm^{-1}. The extra band in dolomite RS spectrum at 1,441 cm^{-1} is due to ν3 asymmetric stretching vibrations of CO_3 group (Gunasekaran et al. 2006). Phlogopite shows its marker bands at 681, 654, 362 and 191 cm^{-1}. Its strongest Raman band found at *ca.* 680 cm^{-1} due to vibrational Si–O–Si mode is diagnostic of trioctahedral phyllosilicates (Tlili et al. 1989; Wang et al. 2015). The other intense and sharp peak at 191 cm^{-1} is attributed to a translational mode of M–O group (vide Singha & Singh 2016).

The presence of magnetite is marked by three marker bands at 668 (A1g), 546 (T2g) and 307 (Eg) cm^{-1} (Fig. 5A). Their positions well agree with literature (e.g., de Faria et al. 1997; Hanesch 2009). Titanium oxides are represented by rutile as evidenced by its bands at 611, 446 and 243 cm^{-1} (Fig. 5D). The first-

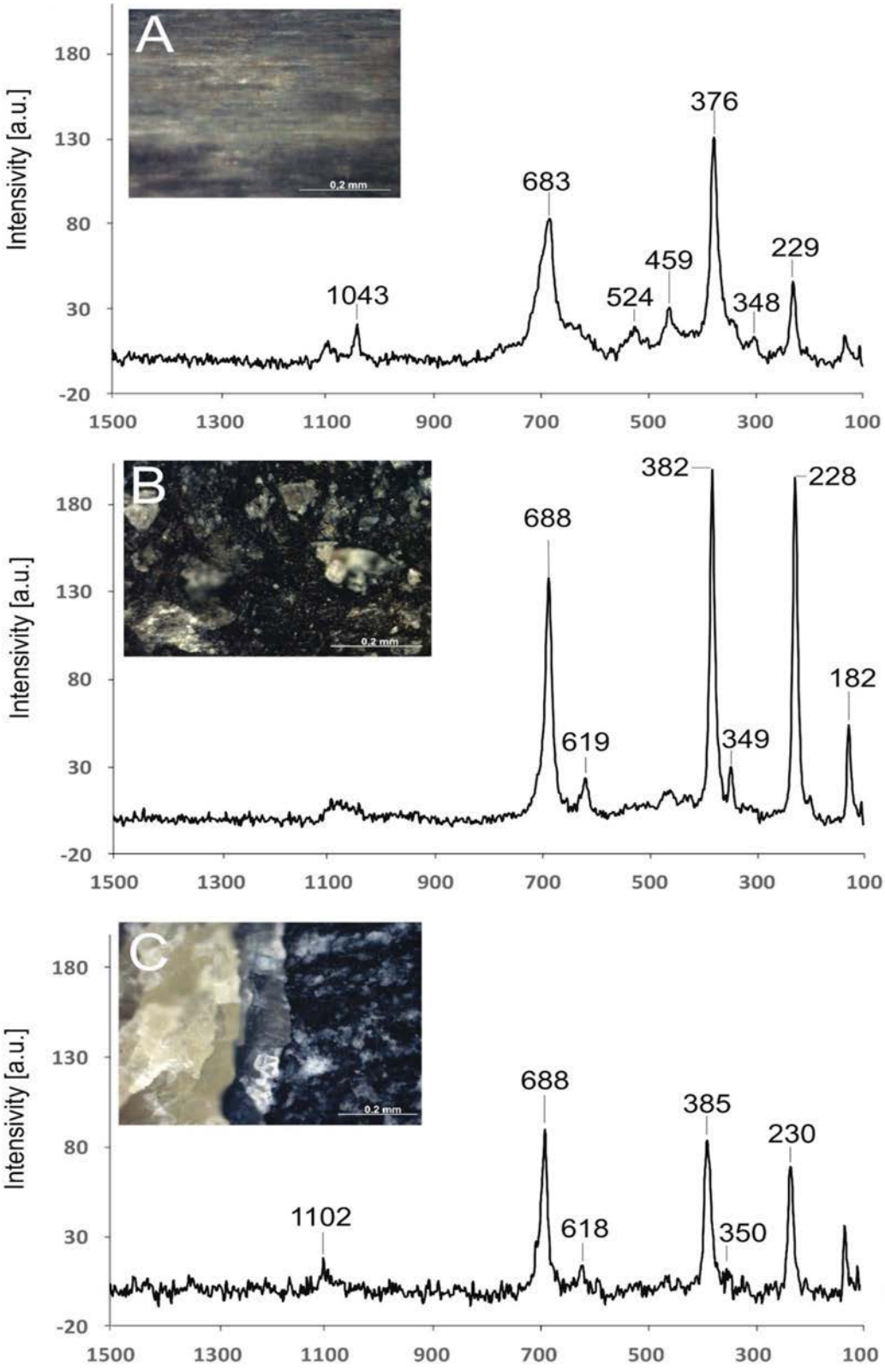

Fig. 4. Raman vibration spectra of serpentine-group minerals from Kon Tum Massif. A. antigorite; B. lizardite; C. chrysotile (sample: LK1/61).

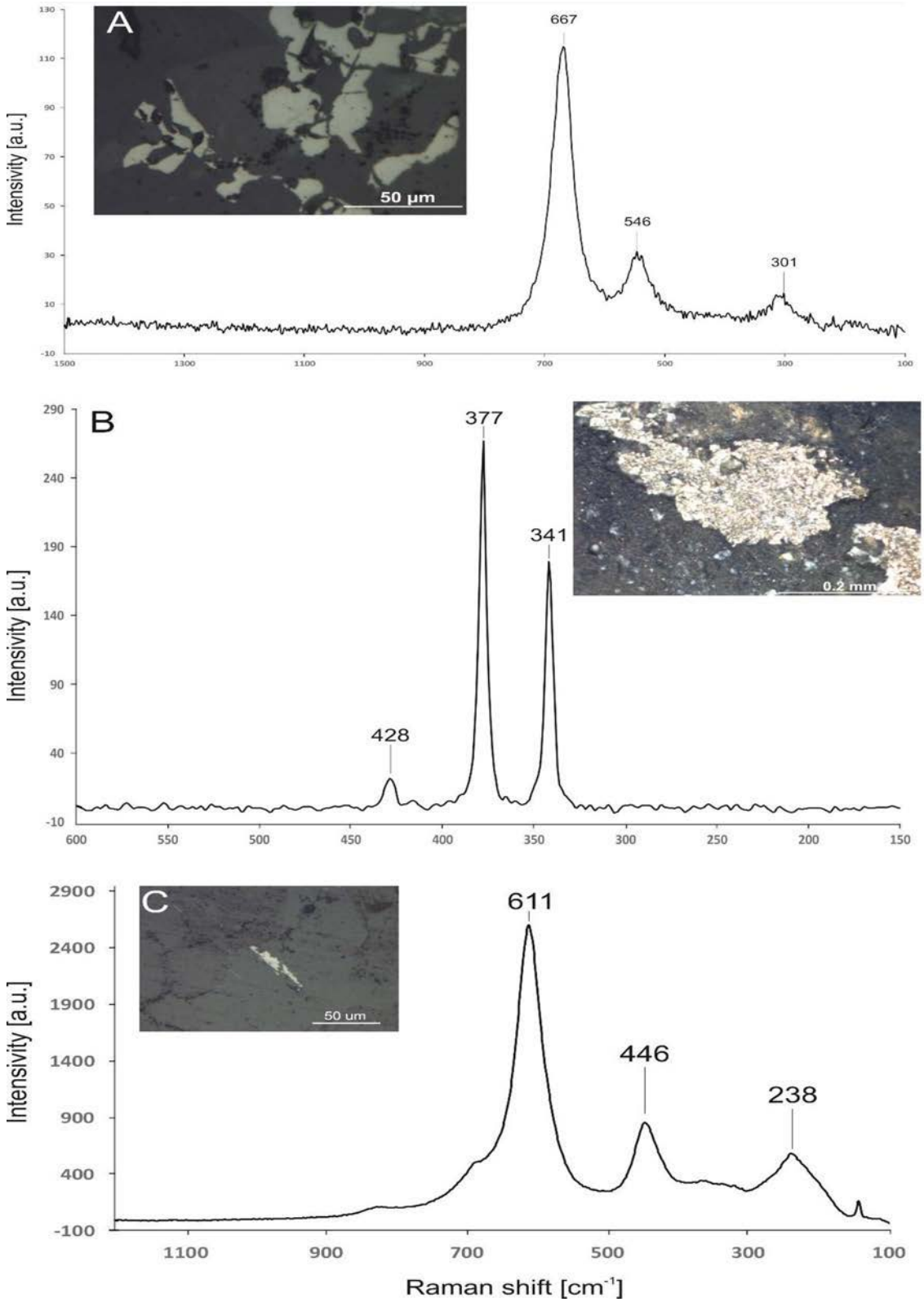

Fig. 5. Raman vibration spectra of accessory ore minerals from Kon Tum Massif. A. magnetite; B. pyrite; C. rutile (sample: LK1/61).

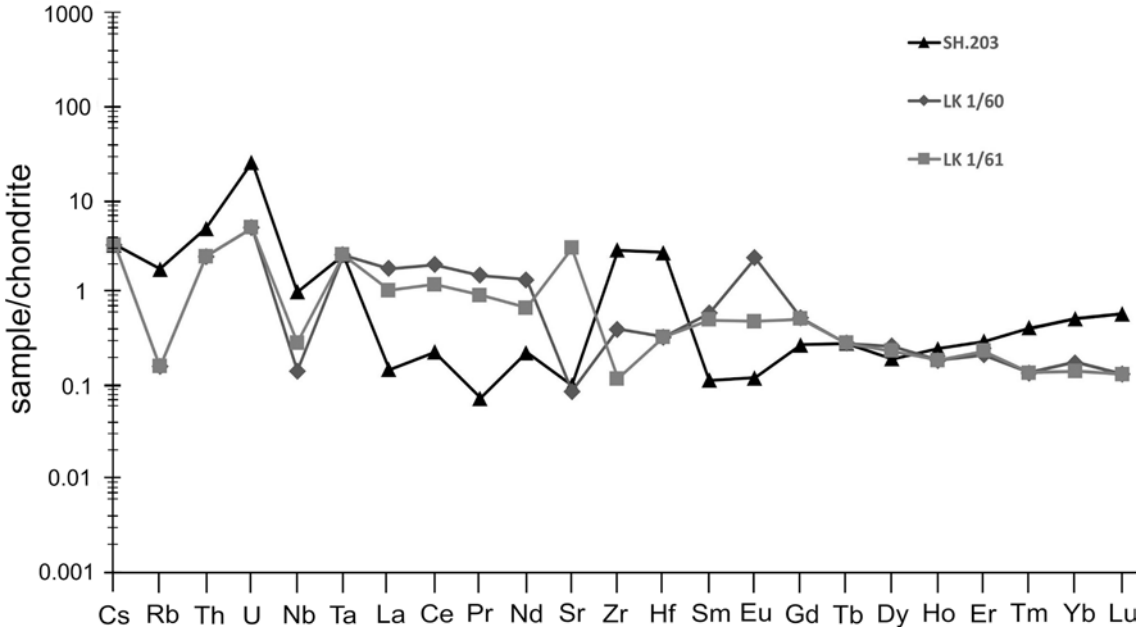

Fig. 6. Multielement pattern of serpentinized ultramafic rocks from Kon Tum Massif (values were normalized to theoretical primary mantle composition after McDonough & Sun 1995).

order Raman-active modes are assigned to A1g, Eg and B1g modes, respectively (Swamy et al. 2006). The presence of pyrite is clearly marked by bands at 428, 378 and 342 cm^{-1} (Fig. 5B). The two most intensive lines at 378 and 342 cm^{-1} are due to Ag and Eg modes, respectively (Kleppe & Jephcoat 2004).

5.4. Whole rock chemistry

Serpentinites from the Sa Nghia area (LK1/60, LK1/61, SH.203) are characterized by low contents of SiO_2 (36.46–41.90 wt.%) (Table 1). They have low to medium contents of CaO (0.06–5.28 wt.%), and high abundances of MgO (37.96–41.20 wt.%). The amounts of Al_2O_3 range from 0.04 to 1.9 wt.%. Their normative mineralogy calculated from chemical data plotted on Ol–Cpx–Opx IUGS ternary diagram (vide Streckeisen 1974) indicated for harzburgite or verhlite affinity of protolith.

The trace elements show low concentration of Cr, Ni, Cu, V, selective depletion in the Ba, K and Ti, and enrichment in Cs, Th and U. (Fig. 6). The positive Zr anomaly was ascertained only for SH.203 sample (coming from surface outcrop). The serpentinites are characterized by constant Y/Nb ratio equalling 1.0 (Table 2). The determined concentrations of REE are presented on Table 3. On multielement patterns, with values normalized to mantle composition, it can be noticed the predominance of LREE over HREE for LK1/60 and LK1/61 samples (Fig. 7). On the other hand, the shape of REE profile line for the sample SH.203 is quite different. It characterized by light LREEs depletion and strong enrichment in HREEs (Fig. 7).

6. Discussion

The serpentinite-bearing marbles, characterized by very attractive and beautiful drawings of their polished surfaces, are found in the Sa Nghia area (Kham Duc Complex, the Kon Tum Massif). Their mineral composition responsible for colours as well as textural features made they are interesting decorative material for local handicraft workshops. The geological and pe-

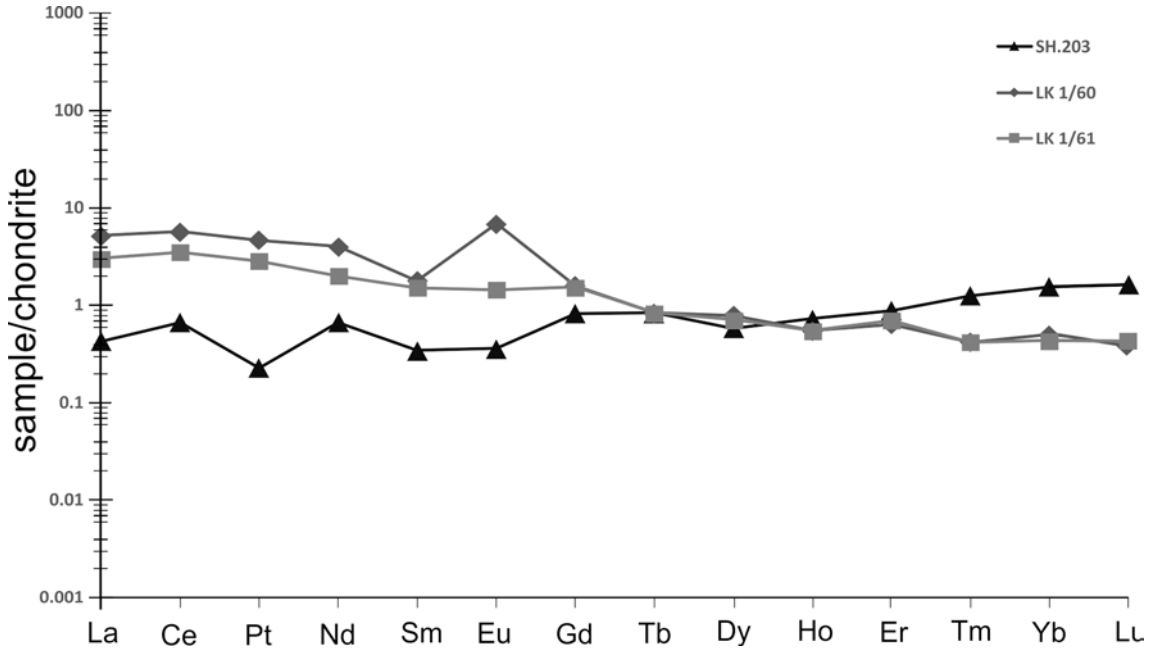

Fig. 7. REE contents in the serpentinized ultramafic rocks from Kon Tum Massif (values were normalized to theoretical primary mantle composition after McDonough & Sun 1995).

trographic details of these ornamental rocks were previously described by Huynh et al. (2009) and Giang et al. (2013). In our contribution these rocks were studied in the context of their origin (protolith) and possible reconstruction of tectono-metamorphic events.

The metacarbonates hosting serpentinite bodies were strongly affected by contact metamorphism and overprinted by hydrothermal changes. Primary dolomites of serpentine marbles were likely to be dedolomitized. Hence, as a result calcite-brucite-serpentine marbles were created. This is well evidenced by the presence of calcite pseudomorphs after dolomite, surrounded by aggregates of oxides of Fe and Mn, i.e., elements that originally could be found as isomorphic substitutions of Ca and Mg ions in dolomites. Furthermore, the presence of wollastonite and actinolite, i.e., minerals characteristic of amphibolite-hornfels facies, seems to prove this theory. The process of dedolomitization was possible under the conditions of this facies, since $MgCO_3$ and $CaCO_3$ dissociate at 402 °C and 898 °C, respectively. The released ions of Mg could be consumed by brucite, or together with silica could enter into the structure of newly formed chrysotile and lizardite. With the increasing temperature, the crystallization of amphiboles (actinolite), wollastonite and garnet could proceed. On the other hand, numerous talc and brucite crystals with minor zincite, indicate the influence of hydrothermal processes. According to actual petrology state of knowledge, wollastonite is a product of following reaction: $CaCO_3$ (calcite) + SiO_2 (quartz) = $CaSiO_3$ (wollastonite) + CO_2 (fluid) which took place during prograde contact metamorphism at relatively low pressure conditions (Ferry et al. 2001). On the other hand, its presence could also indicate the relict phase of granulite facies of the regional metamorphism (T = 850 °C, P = 0.7 GPa; e.g. Ferry et al. 2001). Then, during retrogression, the crystallization of the first generation of serpentine (antigorite) took place at T_{max} = 550 °C and P = 0.4 GPa conditions, which was subsequently replaced and cut by the second generation of serpentines, i.e. lizardite and chrysotile. They could be formed at T = 250 °C and P = 0.2 GPa (e.g. Nance et al. 2006; Keppie et al. 2008; González-Mancera et al. 2009). The next stage of metamorphic transformations, mobilized by CO_2 rich fluids, resulted in the formation of secondary tremolite and phlogopite (Smoliński et al. 2017).

Serpentinite enclaves hosted by metacarbonates, having interpenetrating texture are typical for metamorphic changes, i.e., recrystallization of antigorite

during conditions of early stage of amphibolite facies of regional metamorphism (Wicks & Whittaker 1975). This texture could be interpreted as having been formed by retrograde metamorphism during exhumation of serpentinites, with previously non-pseudomorphic textures (González-Mancera et al. 2009). Ulmer & Trommsdorff (1995) proved that antigorite is the most stable mineral at high pressures, moderate temperatures in the subduction zones. The non-pseudomorphic textures of serpentinites could be ascribed to the original mantle peridotite, before their first serpentinization event. Other microtextures such as "disturbed serpentine veins" or "cell-shaped forms" are typical of lizardite or chrysotile, locally identified in serpentinites of the Sa Nghia area. They might be produced during a late stage of their transformations by hydrothermal activity of low-temperature fluids. The serpentinization events represented by replacement of antigorite by lizardite and chrysotile could occur at 250–350 °C, and pressure conditions of about 2 kbar corresponding to the "main" stage of exhumation of the orogen (Nance et al. 2006; Keppie et al. 2008; Goynzález-Manycera et al. 2009).

The smoothly surrounded grains of zircon being completely homogenous under BSE imagining could be interpreted both as a result of metasomatism of ultramafic rocks in the mantle (Grieco et al. 2001) as well as modified, recrystallized crystals (Corfu et al. 2003). Carbonates in these rocks form different sizes of isolated crystals or fill the interstices between the lamellar antigorite making the main mass of the rocks. They also fill veins crosscutting these rocks. Many carbonate crystals are strongly deformed and fractured, which could result from dynamic activity in this area. The numerous ore minerals associations as well as strongly deformed phlogopite flakes closely coexist with carbonates veins. Simultaneously, the occurrences of brucite along with low-Fe lizardite and magnetite indicate the late stage of serpentinization of these rocks. Pyrite as well as talc and brucite seem to represent hydrothermal products (Keith et al. 2018). Such rich mineral assemblage together with the textural characteristics could indicate a complex alteration history of serpentinites from the Sa Nghia area.

The normative mineralogy calculated from the bulk-rock analyses corresponds to a primary harzburgite (or wehrlite). Poor- or middle-elevated contents of CaO (0.06–5.28 wt.%) and high abundances of MgO (37.96 –301 41.20 wt.%) (Table 1) suggest that CaO is highly mobile, and its depletion could suggest that alteration of clinopyroxene was accompanied by dissolution of Ca (Hattori & Stéphane 2007). This is characteristic of residual peridotites, which final phase equilibrium was reached after removal of the original melt of tholeiitic basalt composition. On the other hand, the amount of Al_2O_3 (0.04, 0.31 and 1.9 wt.%) is typical of low-Al types, possibly more characteristic of magnesium carbonate rocks than residual peridotites (Posukhova et al. 2013). Moreover, the observed linear trends in the distribution of analytical points in two-component systems, i.e., LOI vs MgO, LOI vs CaO and LOI vs SiO_2 indicate a substantial mobility of main oxides during the serpentinization, carbonation and silicification of the protolith.

Most of the trace elements (e.g. Cr, Ni, Cu, V and others; Table 2) occur in much lower abundances than the average values reported for spinel peridotites. Especially controversial is low contents of Cr and Ni, which seem to be more typical for serpentinites of metasomatic than ultramafic origin (Posukhova et al. 2013). The relatively constant Y/Nb ratio ca 1.0 (Table 3) indicates that primary ultramafic rocks could be equilibrated in the spinel peridotites stability field (Leliwa-Kopistyński & Bakun-Czubarow 1983). The distribution of lithophile trace elements normalized to primitive upper mantle (McDonough & Sun 1995) indicates the relative enrichment in Cs, Th and U and impoverishment in Ba, K and Ti (Fig. 6). Such concentration of trace elements could not be associated with seawater alteration of fluids (Stalder et al. 1998).

The contents of REE in serpentinites are variable (Table 3). Their composition normalized to the primary Earth mantle show slight enrichment in LRRE compared to HREE concentrations in samples LK1/60 and LK1/61 (Fig. 7). The REE pattern of samples LK1/61 has an approximately horizontal line profile (on the pattern level), and then progressive depletion in HREE. This LREE enrichment with respect to the HREE contents is probably the effect of metasomatism during subduction and metamorphic interaction with the continental crust (González-Mancera et al. 2009). The profile line of the sample SH.203 exhibits zig-zag course. It shows the depletion in LREEs, and gradual slight increase in HREEs (Fig. 7). The Ce_{CHN}/Yb_{CHN} ratio seems to be typical for residual spinel peridotites as a potential protolith for serpentinites (Loubet et al. 1975). Due to the considerable modification of the protolith of serpentinites, caused by progressive serpentinization and shear deformations, the determination of the origin nature of serpentinite bodies within the carbonates rocks still seems to be challenging

task. Undoubtedly, the rocks were strongly overprinted by metasomatism. Hence, is difficult to state clearly whether these rocks are fragments originating from one distant massif of ultramafic rocks, which were transported into the silicate-carbonate rocks before or after its various transformations. However, field observations, supported by the presence of numerous veins of carbonates accompanied not only by magnetite, but also pyrite, rounded homogenous zircon, as well as bulk-rock chemistry (especially elements such as Al, Cr, Ni, Cu, Co), seem to indicate the strong influence of metasomatic solutions activated in near-surface of the Earth conditions in Sa Nghia area of Kham Duc Complex in Kon Tum Massif.

7. Conclusions

Based on the analytical study, probable model for the development of serpentinization in the Sa Nghia area could be developed as follows:

1. Transformation of primary peridotites during regional metamorphism into antigorite serpentinites in conditions of middle amphibolite facies (T_{max} = 550 °C, P_{max} up to 3 kbar);
2. Retrogressive changes of the antigorite serpentinites during exhumation from deeper crustal levels and formation of chrysotile and lizardite serpentinites (T_{max} = 350 °C, P_{max} = 0.5 kbar);
3. Metamorphism in the shearing zone, resulted of mechanic mixing of the serpentinites with carbonate rocks. The formation of carbonate-serpentine rocks and tremolite schists;
4. The ductile recrystallization event during the late stages of orogen folding. Formation of carbonate veins within the serpentinites and the lizardite veins "overflowing" carbonates.

Acknowledgments

Our thanks go to Sebastian Weber for his detailed comments, which helped to improve the first version of our manuscript. Dr. Uwe Kroner, the editor of Neues Jahrbuch für Geologie und Paläontologie is also acknowledged for the processing of the paper. The work was financially supported by AGH University of Science and Technology (Krakow Poland), grants No 16.16.140.315 and No 15.11.140.209.

References

Azer, M.K. & Khalil, A.E.S. (2005): Petrological and mineralogical studies of Pan-African serpentinites at Bir Al-Edeid area, central Eastern Desert, Egypt. – Journal of African Earth Sciences, **43** (5): 525–536. doi: 10.1016/j.jafrearsci.2005.09.008

Braterman, P.S. & Cygan, R.T. (2006): Vibrational spectroscopy of brucite: A molecular simulation investigation. – American Mineralogist, **91** (7): 1188–1196. doi: 10.2138/am.2006.2094

Brookfield, M.E. (1996): Paleozoic and Triassic Geology of Sundaland. – In: Moullade, M. & Narin, A.E.M. (eds.): The Palaeozoic, B. The Phanerozoic geology of the world I. Amsterdam, Elsevier, 183–264.

Cannat, M., Fontaine, F. & Escartin, J. (2010): Serpentinization and associated hydrogen and methane fluxes at slow spreading ridges. – Diversity of hydrothermal systems on slow spreading ocean ridges, 241–264.

Carter, A., Roques, D., Bristow, C. & Kinny, P. (2001): Under-standing Mesozoic accretion in Southeast Asia: Significance of Triassic thermotectonism (Indosinian orogeny) in Vietnam. – Geology, **29**: 211–214. doi: 10.1130/0091-7613(2001)029<0211:UMAISA>2.0.CO;2

Coleman, R.G. (1977): Ophiolites. – Berlin, Springer, 229 p. doi: 10.1007/978-3-642-66673-5

Corfu, F., Hanchar, J.M., Hoskin, P.W. & Kinny, P. (2003): Atlas of zircon textures. – Reviews in mineralogy and geochemistry, **53** (1): 469–500. doi: 10.2113/0530469

De Faria, D.L.A., Silva, V.S. & De Oliveira, M.T. (1997): Raman microspectroscopy of some iron oxides and oxyhydroxides. – Journal of Raman Spectroscopy, **28**: 873–878. doi: 10.1002/(SICI)1097-4555(199711)28:11<873::AID-JRS177>3.0.CO;2-B

Ferry, J.M., Wing, B.A. & Rumble, D. (2001): Formation of wollastonite by chemically reactive fluid flow during contact metamorphism, Mt. Morrison pendant, Sierra Nevada, California, USA. – Journal of Petrology, **42** (9): 1705–1728. doi: 10.1093/petrology/42.9.1705

Fryer, P., Wheat, C.G. & Mottl, M.J. (1999): Mariana blueschist mud volcanism: Implications for conditions within the subduction zone. – Geology, **27** (2): 103–106. doi: 10.1130/0091-7613(1999)027<0103:MBMVIF>2.3.CO;2

Giang, N.K. (2005): Some preliminary studying results of regolith on ultramafic rocks in Central part of Vietnam. – The Scientific and Technological Journal of Mining and Geology, **9**: 14–21.

Giang, N.K., Dung, L.T. & Van Anh, P.T. (2013): Preliminary studying results of Decorative (Carving) Stones in Kon Tum province. – The Proceedings of the Conference of Technological Universities, Da Lat City, 41–50.

Golonka, J., Krobicki, M., Pająk, J., Nguyen, V.G. & Zuchiewicz, W. (2006): Global plate tectonics and paleogeography of Southeast Asia. – Faculty of Geology, Geophysics and Environmental Protection, AGH University of Science and Technology, Arkadia, Krakow, Poland.

González-Mancera, G., Ortega-Gutiérrez, F., Proenza, J.A. & Atudorei, V. (2009): Petrology and geochem-

istry of Tehuitzingo serpentinites (Acatlán Complex, SW Mexico). – Bolletín de la Sociedad Geológica Mexicana, **61** (3): 419–435. doi: 10.18268/BSGM2009v61n3a9

Grieco, G., Ferrario, A., Von Quadt, A., Koeppel, V. & Mathez, E.A. (2001): The zircon-bearing chromitites of the phlogopite peridotite of Finero (Ivrea Zone, Southern Alps): evidence and geochronology of a metasomatized mantle slab. – Journal of Petrology, **42** (1): 89–101. doi: 10.1093/petrology/42.1.89

Guillot, S. & Hattori, K. (2013): Serpentinites: essential roles in geodynamics, arc volcanism, sustainable development, and the origin of life. – Elements, **9** (2): 95–98. doi: 10.2113/gselements.9.2.95

Gunasekaran, S., Anbalagan, G. & Pandi, S. (2006): Raman and infrared spectra of carbonates of calcite structure. – Journal of Raman Spectroscopy, **37**: 892–899. doi: 10.1002/jrs.1518

Gunia, T. (2005): Geological position of the Sowie Góry block and its influence on the paleogeography of the Paleozoic of Central Sudetes. – Geologia Sudetica, **20** (2): 83–119.

Hai, T.Q. (1986): Precambrian stratigraphy in Indochina: geology of Kampuchea, Laos and Vietnam. – Hanoi, Science Publisher, 20–30.

Hanesch, M. (2009): Raman spectroscopy of iron oxides and (oxy)hydroxides at low laser power and possible applications in environmental magnetic studies. – Geophysical Journal International, **177**: 941–948. doi: 10.1111/j.1365-246X.2009.04122.x

Hattori, K.H. & Stéphane, G. (2007): Geochemical character of serpentinites associated with high- to ultrahigh-pressure metamorphic rocks in the Alps, Cuba, and the Himalayas: Recycling of elements in subduction zones. – Geochemistry, Geophysics, Geosystems, **8** (9). doi: 10.1029/2007GC001594

Hieu, P.T., Dung, N.T., Nguyen, T.B.T., Minh, N.T. & Minh, P. (2016): U–Pb ages and Hf isotopic composition of zircon and bulk rock geochemistry of the Dai Loc granitoid complex in Kontum massif: Implications for early Paleozoic crustal evolution in Central Vietnam. – Journal of Mineralogical and Petrological Sciences, **111** (5): 326–336. doi: 10.2465/jmps.151229

Hirth, G. & Guillot, S. (2013): Rheology and tectonic significance of serpentinite. – Elements, **9** (2): 107–113. doi: 10.2113/gselements.9.2.107

Hutchison, C.S. (1989): Geological evolution of Southeast Asia. – Oxford Clarendon Press, **13**: 368.

Huynh, T., Tran, P.H., Le, D.P., Nguyen, K.H., Tran, D.T. & Truing, C.C. (2009): Geological characteristics and forming origin of ultramafic rocks (serpentinite) of Hiep Duc complex. – J. Sci. Dev., VNU-HCMC, **12** (10): 89–98.

Katz, M.B. (1993): The Kannack complex of the Vietnam Kontum Massif of the Indochina Block: an exotic fragment of Precambrian Gondwanaland. – Gondwana, **8**: 161–164.

Keith, M., Smith, D.J., Jenkin, G.R., Holwell, D.A. & Dye, M.D. (2018): A review of Te and Se systematics in hydrothermal pyrite from precious metal deposits: Insights into ore-forming processes. – Ore Geology Reviews, **96**: 269–282. doi: 10.1016/j.oregeorev.2017.07.023

Keppie, J.D., Dostal, J., Murphy, J.B. & Nance, R.D. (2008): Synthesis and tectonic interpretation of the westernmost Paleozoic Variscan orogen in southern Mexico: From rifted Rheic margin to active Pacific margin. – Tectonophysics, **461** (1–4): 277–290. doi: 10.1016/j.tecto.2008.01.012

Kleppe, A.K. & Jephcoat, A.P. (2004): High-pressure Raman spectroscopic studies of FeS_2 pyrite. – Mineralogical Magazine, **68** (3): 433–441. doi: 10.1180/0026461046830196

Lan, C.Y., Chung, S.L., Long, T.V., Lo, C.H., Lee, T.Y., Mertzman, S.A. & Shen, J. (2003): Geochemical and Sr-Nd isotopic constrains from the Kontum massif, central Vietnam on the crustal evolution of the Indochina block. – Precambrian Research, **122**: 7–27. doi: 10.1016/S0301-9268(02)00205-X

Leliwa-Kopiński, J. & Bakun-Czubarow, N. (1983): Phase transitions in Earth's mantle. Physics and evolution of Earth interior. – In: Teisseyre, R. (ed.): PWN, **1**: 178–206 (in Polish).

Lepvrier, C., Maluski, H., Thich, V.V., Leyreloup, A., Thi, P.T. & Nguyen, V.V. (2004): The Early Triassic Indosinian orogeny in Vietnam (Truong Son Belt and Kontum Massif): implications for the geodynamic evolution of Indochina. – Tectonophysics, **393**: 87–118. doi: 10.1016/j.tecto.2004.07.030

Loubet, M., Shimizu, N. & Allegre, C.J. (1975): Rare earth elements in alpine peridotites. – Contributions to Mineralogy and Petrology, **53** (1): 1–12. doi: 10.1007/BF00402450

Maluski, H., Lepvrier, C., Leyreloup, A., Van Tich, V. & Thi, P.T. (2005): ^{40}Ar–^{39}Ar geochronology of the charnockites and granulites of the Kan Nack complex, Kon Tum Massif, Vietnam. – Journal of Asian Earth Sciences, **25** (4): 653–677. doi: 10.1016/j.jseaes.2004.07.004

McDonough, W.F. & Sun, S.S. (1995): The composition of the Earth. – Chemical Geology, **120** (3–4): 223–253. doi: 10.1016/0009-2541(94)00140-4

Metcalfe, I. (1984): Stratigraphy, paleontology and paleogeography of the Carboniferous of Southeast Asia, Tethys. – Mémoire de la Société Géologique de France, **147**: 107–118.

Metcalfe, I. (1988): Origin and assembly of Southeast Asian 461 continental terranes. – In: Audley-Charles, M.G. & Hallam, A. (eds.): Gondwana and Tethys, Geological Society of London Special Publication, **37**: 101–118.

Metcalfe, I. (1994): Late Paleozoic and Mesozoic paleogeography of Eastern Pangea and Tethys. – In: Embry, A.F., Beauchamp, B. & Glass, D.J. (eds.): Pangea: global environments and resources. Canadian Society of Petroleum Geologists Memoir, **17**: 97–111.

Metcalfe, I. (1996): Gondwanaland dispersion, Asian accretion and evolution of eastern Tethys. – Australian Journal of Earth Sciences, **43** (6): 605–623. doi: 10.1080/08120099608728282

Metcalfe, I. (1998): Palaeozoic and Mesozoic geological evolution of the SE Asian region: multidisciplinary constraints and implications for biogeography. – Biogeography and geological evolution of SE Asia, 25–41.

Metcalfe, I. (2000): The Bentong-Raub suture zone. – Journal of Asian Earth Sciences, **18** (6): 691–712. doi: 10.1016/S1367-9120(00)00043-2

Nagy, E.A., Maluski, H., Lepvrier, C., Schärer, U., Thi, P.T., Leyreloup, A. & Thich, V.V. (2001): Geodynamic significance of the Kontum massif in central Vietnam: composite $^{40}Ar/^{39}Ar$ and U-Pb ages from Paleozoic to Triassic. – The Journal of Geology, **109**: 755–770. doi: 10.1086/323193

Nakano, N., Osanai, Y. & Owada, M. (2007a): Multiple breakdown and chemical equilibrium of silicic clinopyroxene under extreme metamorphic conditions in the Kontum Massif, central Vietnam. – American Mineralogist, **92** (11–12): 1844–1855. doi: 10.2138/am.2007.2478

Nakano, N., Osanai, Y., Owada, M., Nam, T.N., Toyoshima, T., Binh, P., Tsunogae, T. & Kagami, H. (2007b): Geologic and metamorphic evolution of the basement complexes in the Kontum Massif, central Vietnam. – Gondwana Research, **12**: 438–453. doi: 10.1016/j.gr.2007.01.003

Nakano, N., Osanai, Y., Owada, M., Nam, T.N., Hayasaka, T. & Tran, N.N. (2009): Permo–Triassic Barrovian-type metamorphism in the ultrahigh-temperature Kontum Massif, central Vietnam: Constraints on continental collision tectonics in Southeast Asia. – Island Arc, **18**: 126–143. doi: 10.1111/j.1440-1738.2008.00646.x

Nance, R.D., Miller, B.V., Keppie, J.D., Murphy, J.B. & Dostal, J. (2006): Acatlán Complex, southern Mexico: record spanning the assembly and breakup of Pangea. – Geology, **34**: 857–860. doi: 10.1130/G22642.1

Osanai, Y., Nakano, N., Owada, M., Nam, T.N., Toyoshima, T., Tsunogae, T. & Binh, P. (2004): Permo-Triassic ultrahigh-temperature metamorphism in the Kontum massif, central Vietnam. – Journal of Mineralogical and Petrological Sciences, Special Issue, **99** (4): 225–241. doi: 10.2465/jmps.99.225

Osanai, Y., Nakano, N., Owada, M., Nam, T.N., Toyoshima, T., Tsunogae, T. & Kagami, H. (2003): Metamorphic and tectonic evolution of the Kontum Massif, Vietnam. – Earth monthly, **25**: 244–251.

Owada, M., Osanai, Y., Nakano, N., Adachi, T., Kitano, I., Van Tri, T. & Kagami, H. (2016): Late Permian plume-related magmatism and tectonothermal events in the Kontum Massif, central Vietnam. – Journal of Mineralogical and Petrological Sciences, **111** (3): 181–195. doi: 10.2465/jmps.151019b

Phan, T.T. (1978): Stratigraphy and petrology of the Precambrian formations of Vietnam. – Soviet Geology and Geophysics. **19**: 31–37.

Posukhova, T.V., Panasian, L.L. & Sas, I.E. (2013): Serpentinites of the Ural: Mineralogical Features, Petrophysical Properties and Subduction Processes. – Open Journal of Geology, **3** (3): 250. doi: 10.4236/ojg.2013.33029

Singha, M. & Singh, L. (2016): Vibrational spectroscopic study of muscovite and biotite layered phyllosilicates. – Indian Journal of Pure & Applied Physics, **54**: 116–122.

Smoliński, W., Gunia, P., Natkaniec-Nowak, L., Giang, N.K., Dumańska-Słowik, M., Heflik, W., Pham Thi, V.A. & Gola, M. (2017): Serpentine-Wollastonite rocks from Sa Nghĩa (Kon Tum, Central Vietnam) – preliminary results. – Mineralogicko petrologická konferencia Petros 2017, Book of Abstracts: 56–57.

Stalder, R., Foley, S.F., Brey, G.P. & Horn, I. (1998): Mineral-aqueous fluid partitioning of trace elements at 900–1200 °C and 3.0–5.7 GPa: new experimental data for garnet, clinopyroxene, and rutile, and implications for mantle metasomatism. – Geochimica et Cosmochimica Acta, **62** (10): 1781–1801. doi: 10.1016/S0016-7037(98)00101-X

Streckeisen, A. (1974): Classification and nomenclature of plutonic rocks recommendations of the IUGS subcommission on the systematics of igneous rocks. – Geologische Rundschau, **63** (2): 773–786. doi: 10.1007/BF01820841

Swamy, V., Muddle, B.C. & Dai, Q. (2006): Size-dependent modifications of the Raman spectrum of rutile TiO_2 Citation. – Applied Physics Letters, **89**: 163118. doi: 10.1063/1.2364123

Tlili, A., Smith, D., Beny, J. & Boyer, H. (1989): A Raman microprobe study of natural micas. – Mineralogical Magazine, **53**: 165–179. doi: 10.1180/minmag.1989.053.370.04

Tran, N.N. (1998): Thermotectonic events from Early Proterozoic to Miocene in the Indochina craton: implication of K-Ar ages in Vietnam. – Journal of Asian Earth Sciences, **19**: 77–84.

Trinh, V.L. (1995): Paired metamorphic belts of Kham Duc complex. – Journal of Geology of Hanoi, **11**: 2.

Ulmer, P. & Trommsdorff, V. (1995): Serpentine stability to mantle depths and subduction-related magmatism. – Science, **268** (5212): 858–861, 82–292.

Wang, A., Freeman, J.J. & Jolliff, B.L. (2015): Understanding the Raman spectral features of phyllosilicates. – Journal of Raman Spectroscopy, **46**: 829–845. doi: 10.1002/jrs.4680

Wicks, F.I. & Whittaker, E.J.W. (1975): A reappraisal of the structures of the serpentine minerals. – Canadian Mineralogist, **13**: 227–243.

Yang, K. & Seccombe, P.K. (1993): Platinum-group minerals in the chromitites from the Great Serpentinite Belt, NSW, Australia. – Mineralogy and Petrology, **47** (2–4): 263–286.

Manuscript received: January 27th, 2020.
Revised version accepted by the Freiberg editor: July 7th, 2020.

Addresses of the authors:

Wojciech Smoliński, Lucyna Natkaniec-Nowak (corresponding author), Wiesław Heflik, Magdalena Dumańska-Słowik, Faculty of Geology, Geophysics and Environmental Protection, AGH-University of Science and Technology;
e-mail: natkan@agh.edu.pl

Giang Nguyen Khac, Ban To Xuan, Faculty of Geosciences and Geoengineering, Hanoi University of Mining and Geology, Hanoi, Vietnam.

Piotr Gunia, Institute of Geological Sciences, Mineralogy and Petrology Department, University of Wroclaw, Wroclaw 50-205, 9 Max Born Sq.

Table 1. Bulk-rock chemistry of the Kon Tum serpentinites and accompanied metacarbonate rocks (in wt.%). * total Fe content is expressed as Fe_2O_3.

lp	1	2	3	4
Sample symbol	**LK 1/61**	**LK 1/67**	**LK 2/40**	**SH.203**
SiO_2	41.90	36.46	25.39	38.36
TiO_2	0.02	0.01	0.01	0.11
Al_2O_3	0.04	0.31	0.13	1.9
Fe_2O_3	1.64*	0.88*	4.65*	1.60*
FeO	–	–	–	–
MnO	0.05	0.05	0.13	0.05
MgO	41.20	37.96	31.14	40.03
CaO	0.06	5.28	11.73	0.18
Na_2O	<0.01	<0.01	<0.01	<0.01
K_2O	<0.01	<0.01	<0.01	<0.01
P_2O_5	0.01	<0.01	<0.01	<0.01
LOI	15.0	19.0	26.3	17.1
Total	99.94	99.98	99.51	99.36
CIPW normative composition (% vol.)				
Olivine	63.99	83.63	65.33	72.80
Hypersthene	35.87	–	–	27.20
Diopside (DiCa-silicate)	0.14	16.37	(17.91)	–
Protolith	Harzburgite	Werhlite?	Calcsilicate rock?	Harzburgite

Table 2. Trace elements chemistry of the Kon Tum serpentinites and accompanied meta-carbonate rocks (in ppm).

lp	1	2	3	4
Sample symbol	**LK 1/61**	**LK 1/67**	**LK 2/40**	**SH.203**
As	1.2	1.7	0.9	0.7
Ag	<0.1	<0.1	<0.1	<0.1
Au(ppb)	0.5	0.6	<0.5	<0.5
Ba	<1	<1	<1	1
Be	<1	<1	<1	<1
Bi	<0.1	<0.1	<0.1	<0.1
Cs	<0.1	<0.1	<0.1	<0.1
Cd	0.1	<0.1	<0.1	<0.1
Co	1.2	0.3	0.8	1.5
Cr	<15	<15	<15	<15
Cu	0.5	1	4.4	0.8
Ga	<0.5	<0.5	<0.5	0.6
Hf	0.1	<0.1	<0.1	0.8
Hg	<0.01	<0.01	<0.01	<0.01
Mo	<0.1	<0.1	0.6	0.8
Nb	0.1	0.2	<0.1	0.7
Ni	1.3	1.5	1.3	3.7
Pb	20.5	1.2	2.1	1
Rb	<0.1	<0.1	1.1	1.1
Sb	<0.1	<0.1	<0.1	<0.1
Sc	<1	<1	<1	1
Se	<0.5	<0.5	<0.5	<0.5
Sn	<1	<1	<1	<1
Sr	1.8	60.8	89.6	2.1
Ta	<0.1	<0.1	<0.1	<0.1
Th	<0.2	0.2	0.4	0.4
Tl	<0.1	<0.1	0.1	<0.1
U	<0.1	<0.1	0.2	0.5
V	41	34	9	25
W	1.4	<0.5	0.6	1.2
Y	0.9	1.1	2.7	1.4
Zn	33	9	7	29
Zr	4.4	1.3	4.8	31

Table 3. REE chemistry of the Kon Tum serpentinites and accompanied meta-carbonate rocks (in ppb).

lp	1	2	3	4
Sample symbol	**LK 1/61**	**LK 1/67**	**LK 2/40**	**SH.203**
La	1.20	0.70	1.60	0.10
Ce	3.40	2.10	3.30	0.40
Pr	0.41	0.25	0.42	0.02
Nd	1.80	0.90	1.90	<0.30
Sm	0.26	0.22	0.59	<0.05
Eu	0.38	0.08	0.28	<0.02
Gd	0.31	0.3	0.97	0.16
Tb	0.03	0.03	0.12	0.03
Dy	0.19	0.17	0.62	0.14
Ho	0.03	0.03	0.08	0.04
Er	0.10	0.11	0.23	0.14
Tm	<0.01	<0.01	0.03	0.03
Yb	0.08	0.07	0.16	0.25
Lu	0.01	<0.01	0.01	0.04